INORGANIC CHEMISTRY FRONTIERS

RESEARCH ARTICLE

View Article Online
View Journal | View Issue

Check for updates

Cite this: *Inorg. Chem. Front.*, 2024, **11**, 735

High-pressure observation of elusive iodoplumbic acid in different hydronium-hydrate solid forms†‡

Szymon Sobczak, [a] Athena M. Fidelli,[b] Jean-Louis Do, [b] George P. Demopoulos, *[c] Audrey Moores, *[b] Tomislav Friščić *[b,d] and Andrzej Katrusiak *[a]

Received 13th June 2023,
Accepted 2nd December 2023

DOI: 10.1039/d3qi01102j

rsc.li/frontiers-inorganic

High-pressure and high-temperature isochoric crystallization combined with single-crystal X-ray diffraction revealed the proposed, but previously never demonstrated, hydronium acid hydrates of $[PbI_3]^-$, the closest forms of the elusive iodoplumbic acid. Depending on the pressure range, the reaction of PbI_2 and aqueous concentrated hydriodic acid under isochoric conditions in a diamond anvil cell held between 0.11 and 1.20 GPa produces two hydrated acids with compositions $[H_3O][PbI_3]\cdot nH_2O$ (n = 3, 4). Comprised of polymeric one-dimensional double-chain PbI_3^- anions, analogous to those seen in archetypal lead-halide perovskites such as $RbPbI_3$ and $CsPbI_3$, these hydrates offer the first observation of the iodoplumbic acid progenitor of hybrid lead perovskites. We also reveal the 'hidden' polymorph of lead(II) iodide, adopting a three-dimensional Pb–I bonded network, contrasting with the prototypic ambient-pressure layered PbI_2 structure.

Published on 06 Desemba 2023. Downloaded on 08/10/2025 15:51:46.

Introduction

The emergence of photovoltaic lead halide perovskites $APbI_3$, where A = alkaline metal, ammonium or organoammonium cation has sparked extensive studies on the existence of iodoplumbic(II) acid, $HPbI_3$.[1,2] In most cases, lead halide perovskites are composed of polymeric PbI_3^- anions, such as NH_4PbI_3,[3] $[CH_3NH_3]PbI_3$ [4–9] or $CsPbI_3$,[10–12] which can be synthesized *via* traditional[13] as well as unconventional methods.[14–16] The proposed $HPbI_3$ would be the simplest member of this compound class and the progenitor of hybrid, as well as inorganic lead(II) perovskites. There were several attempts to propose a computational prediction of the most probable $HPbI_3$ structure, which suggested that it forms a 3-dimensional perovskite structure of space-group symmetry $Pm\bar{3}m$, consisting of the PbI_3-polyanionic framework encapsulating hydrogen inside the cubic cages.[17] Whereas iodoplumbic acid was proposed as a precursor for the synthesis of hybrid perovskites in 2015 by Zhao *et al.*,[18] the existence of an acid with composition $HPbI_3$ has remained controversial.[19–28] The groups of Kanatzidis and of Hillebrecht[29,30] have shown that the postulated $HPbI_3$ precipitate obtained from *N*,*N*-dimethylformamide (DMF) solutions of PbI_2 and hydriodic acid (HI) is actually the dimethylammonium hybrid perovskite $[N(CH_3)_2H_2]PbI_3$. Moreover, Daub and Hillebrecht demonstrated that the reaction of PbI_2 with concentrated (57% w/w) aqueous HI can produce two forms of hydrated iodoplumbic acid.[30] One form exhibits the composition $[H_3O]_{2x}[Pb_{1-x}I_2]\cdot(2-2x)H_2O$ (**1**) ($x \approx 0.23$), and is based on two-dimensional (2-D) anionic CdI_2-type sheets with approximate composition $[Pb_3I_8^{2-}]_n$ (Fig. 1a). The second reported form of hydrated iodoplumbic acid exhibits the composition $(H_3O)_2Pb_3I_8\cdot 6H_2O$ (**2**) (Fig. 1b), and is based on one-dimensional (1-D) polyanionic tapes of $[Pb_3I_8^{2-}]_n$.

Compound **2** was reported to be the first product of either crystallization of PbI_2 from concentrated aqueous HI, or of the gas–solid reaction between PbI_2 and HI vapours. When exposed to open air, **2** quickly transforms into **1**. Anions in both **1** and **2** are separated by layers of water molecules containing hydronium ions. Overall, these prior studies suggest that an inorganic acid based on the PbI_3^- anion does not exist, and that the only accessible forms of iodoplumbic acid are hydronium salts of the $Pb_3I_8^{2-}$ anion.

We now report the synthesis and observation of a hydronium salt of $[Pb_2I_6]^{2-}$ achieved under unconventional, isochoric con-

[a]*Department of Materials Chemistry, Faculty of Chemistry, Adam Mickiewicz University, Uniwersytetu Poznanskiego 8, 61-614 Poznań, Poland. E-mail: katran@amu.edu.pl; https://twitter.com/szymon_sobczakhttps://twitter.com/DMCh_AMU*

[b]*Department of Chemistry, McGill University, 801 Sherbrooke St West, Montreal, QC, H3H 0B8, Canada. E-mail: audrey.moores@mcgill.ca; https://twitter.com/MooresResearchhttps://twitter.com/JLD_Chemisthttps://twitter.com/TomislavFriscic*

[c]*Department of Materials Engineering, McGill University, 801 Sherbrooke St West, Montreal, QC, H3A 0C5, Canada. E-mail: george.demopoulos@mcgill.ca*

[d]*School of Chemistry, University of Birmingham, Edgbaston, Birmingham B15 2TT, UK. E-mail: t.friscic@bham.ac.uk*

†Electronic supplementary information (ESI) available. CCDC 2071140–2071144. For ESI and crystallographic data in CIF or other electronic format see DOI: https://doi.org/10.1039/d3qi01102j

‡A previous version of this manuscript has been deposited on a preprint server (https://doi.org/10.26434/chemrxiv.14369813.v1).

Published on 06 Desemba 2023. Downloaded on 08/10/2025 15:51:46.

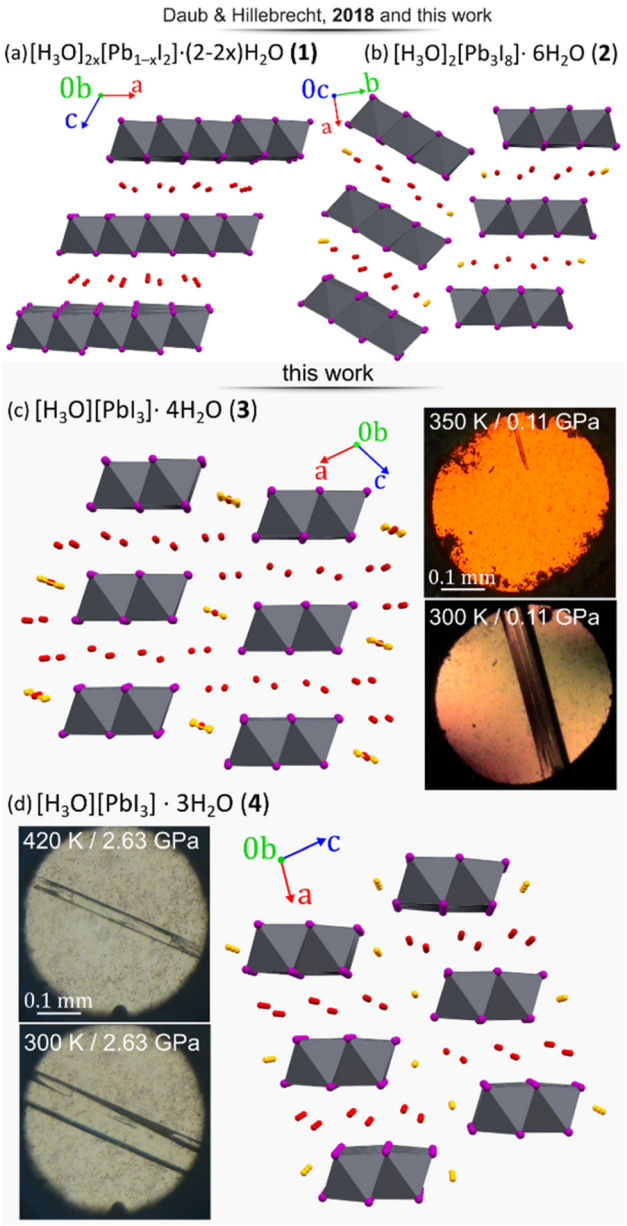

Fig. 1 Four forms of hydrated iodoplumbic acid obtained by reaction of PbI_2 and concentrated aqueous HI: (a) $[H_3O]_{2x}[Pb_{1-x}I_2]\cdot(2-2x)H_2O$ (**1**, $x \approx 0.23$); (b) $(H_3O)_2Pb_3I_8\cdot 6H_2O$ (**2**);[30] as well as new materials herein synthesized under high-pressure (*p*) and -temperature (*T*) conditions: (c) $(H_3O)PbI_3\cdot 4H_2O$ (**3**) and (d) $(H_3O)PbI_3\cdot 3H_2O$ (**4**). The proposed sites of H_3O^+ cations are marked in orange. Photographs show crystals **3** and **4** *in situ* grown under pressure.

ditions of elevated temperature and pressure. Specifically, we show that crystallization of PbI_2 from concentrated aqueous HI provides, at pressure above 0.11 GPa, access to hydronium of 1-D double-chain polyanions with composition PbI_3^-. Based on the chemical and structural composition of the anion, which are identical to those in $RbPbI_3$, $CsPbI_3$ *etc.*, and the absence of any ammonium or metal cations in the system, the herein reported structures can be considered a significant step towards the observation and understanding of iodoplumbic acid, a historically elusive entity.

Results and discussion

With $HPbI_3$ apparently inaccessible by solution techniques, our study has focused on less conventional reaction environments based on introduction of mechanical energy in the form of either ball milling (mechanochemistry)[31–33] or by high-pressure chemistry. Our first exploration of reactivity between PbI_2 and concentrated aqueous hydroiodic acid HI (aq) was done mechanochemically, by milling of the two components in the stoichiometric ratio of PbI_2/HI = 1.5 : 1 (corresponding to the 3 : 8 stoichiometric ratio of Pb to I, respectively). Milling produced a bright yellow powder that, upon powder X-ray diffraction (PXRD) analysis, matched the previously reported **1** (see ESI†). Increasing the amount of HI(aq) in the milling reaction to produce a 1 : 3 respective stoichiometric ratio of PbI_2 and HI led to the formation of **2** in a pure form (see ESI†). Consistent with previous work,[30] upon standing in air **2** slowly transforms into **1** and, subsequently, into the orange solid PbI_2.

A different approach to introduce mechanical energy to a reaction is in the form of hydrostatic pressure in a diamond anvil cell (DAC),[34–40] allowing the exploration of otherwise inaccessible thermodynamic coordinates and formation of new products.[39–42] As a reactor, the DAC represents an almost perfect closed system confining the reaction to the volume of ~0.02 mm^3 between two diamond culets and a steel gasket.[41] For each of the high-pressure reactions, a saturated solution of PbI_2 in HI(aq) was loaded in the DAC and isothermally compressed at 297 K. At 0.11 GPa, a polycrystalline mass precipitated that, upon subsequent isochoric recrystallization led to a colorless elongated prism-shaped crystal suitable for structure determination by single-crystal X-ray diffraction (SCXRD). After increasing pressure to 0.20 GPa, the unit-cell dimensions were determined (see ESI Table S1†) and the next SCXRD measurement at 0.5 GPa revealed a novel hydrated hydronium salt of composition $(H_3O)PbI_3\cdot 4H_2O$ (**3**). The structure of **3** consists of 1-D anionic PbI_3^- tapes of edge-sharing PbI_6-octahedra running along the crystallographic *b*-axis (Fig. 1c). The PbI_6-octahedra in the PbI_3^- polyanion are distorted, exhibiting four different lengths of Pb–I bonds around each metal ion: 3.046 (2), 3.174(6) (twice), 3.250(6) (twice), and 3.3663(19) Å. These Pb–I bond length distances are very similar to those observed in diguanidinium tetraiodoplumbate[43] and other 6-coordinated lead(II) complexes (see ESI, Fig. S10†), confirming the retention of the Pb^{2+} oxidation state. Importantly, the PbI_3^- anionic tapes in **3** are identical to those in $NH_4CdCl_3\cdot 2H_2O$, hybrid and lead iodide perovskites $CsPbI_3$, $RbPbI_3$, as well as related hydrates $NH_4PbI_3\cdot 2H_2O$, $CsPbI_3\cdot 2H_2O$, and $CH_3NH_3PbI_3\cdot H_2O$.[44–49] The structure of the anion makes compound **3** the first example of a direct hydronium-based acid analogue of these well-known lead perovskite solids. Crystallographic parameters for **3** are distinct from those of previously reported[30] **1** or **2** (Fig. 1c and Table 1).

Each $[PbI_3]_n^-$ polyanion requires a counter hydronium cation for the charge balance. Although the strong scattering of X-rays by heavy lead and iodine atoms hinders the precise

 This journal is © the Partner Organisations 2024

Published on 06 Desemba 2023. Downloaded on 08/10/2025 15:51:46.

Table 1 Selected crystallographic data for compounds **1–4** and β-PbI_2. The structure of **1** was re-determined at ambient conditions on a crystal that was obtained by single-crystal-to-single-crystal decomposition of a crystal of **3** and recovered from the DAC

Compound	**1**[a]	**2**[30]	**3**	**4**	β-PbI_2
Formula	$[H_3O]_{0.40}[Pb_{0.6}I_2]\cdot 1.6H_2O$	$(H_3O)_2Pb_3I_8\cdot 6H_2O$	$(H_3O)PbI_3\cdot 4H_2O$	$(H_3O)PbI_3\cdot 3H_2O$	PbI_2
P (GPa)	0.0001	0.0001	0.5	2.63	2.05
T (K)	300	300	300	300	320
Space group	$C2/m$	$Pbam$	$I2/m$	$P2_1/m$	$C2/m$
a (Å)	7.8946(10)	10.033(3)	16.205(2)	9.57(3)	14.06(4)
b (Å)	4.5598(3)	30.126(7)	4.5170(1)	4.513(3)	4.4560(12)
c (Å)	11.1985(18)	4.5610(10)	17.184(14)	12.98(11)	10.540(6)
β (°)	118.023(19)	—	111.50(4)	95.9(6)	93.08(12)
V (Å^3)	355.859	1378.66(6)	1170.3(10)	558(5)	654.9(17)
D_{calc} (g cm^{-3})	4.638	4.290	3.666	3.883	7.013

[a]The herein determined structure $[H_3O]_{2x}[Pb_{1-x}I_2]\cdot(2-2x)H_2O$, $x = 0.20(2)$, is analogous to that previously reported[30] with $x = 0.23$.

location of hydrogen atoms in X-ray diffraction, the location of oxygen atoms and their shortest distances can discriminate the corresponding water molecules and hydronium ions. It is known that the hydronium cations form with iodide anions strong, charge-assisted O···I bonds, significantly shorter that those involving water molecules. In **3**, the $[Pb_2I_6]^{2-}$ polyanions are separated by tapes of hydrogen-bonded water molecules (Fig. 1c and 2b) connected into an extended honeycomb-like structure through O–H···O hydrogen bonds with O···O distances of 2.63(4), 2.68(6) and 2.79(7) Å. The tapes propagate in the crystallographic *b*-direction and are periodically interrupted by iodoplumbate(II) anions, forming I···O contacts that are significantly shorter than the 3.54 Å non-bonding distance expected from the sum of van der Waals radii[50] of O (1.50 Å) and I (2.04 Å) atoms, indicating the formation of the charge-assisted O–H···I bonds. The structure of **3** also exhibits 1-D arrays of oxygen atoms (with O···O distances of 2.41(6) Å) separate from the hydrogen-bonded honeycomb tapes, which are located between pairs of polymeric PbI_3^- anions (Fig. 2b). At 0.50 GPa, these oxygen atoms are situated at notably short I···O distances of 3.2(2) Å, that are commensurate with charge-assisted[51] O–H···I hydrogen bonding, tentatively indicating the location of H_3O^+ ions.

While increasing the pressure up to 1.20 GPa does not affect the crystals of **3**, releasing the pressure to 0.1 MPa quickly leads to their transformation into **1** (Fig. 3). This

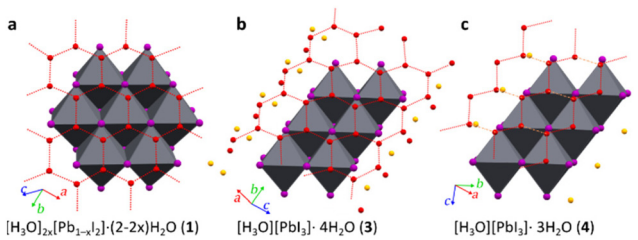

Fig. 2 Fragments of crystal structures of (a) **1** herein re-determined[30] from a crystal obtained by transformation of **3** at 0.1 MPa; (b) **3**; and (c) **4**, all viewed perpendicular to the honeycomb pattern of water molecules (red-dotted lines, orange-dashed lines in **4** mark the longest O···O distances). The oxygen-atom sites suggested for H_3O^+ ions are shown in orange.

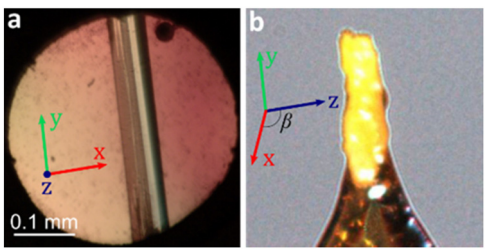

Fig. 3 Single crystal of **3**: (a) as grown in the DAC and (b) after being recovered to ambient conditions and transforming to **1**, mounted on a nylon loop. Crystal axes are indicated.

chemical transformation takes place in a single-crystal-to-single-crystal manner, as shown by X-ray diffraction on the crystal recovered from the DAC (see ESI†), which revealed a clear matrix relationship between the lattices for the starting crystal structure of $H_3OPbI_3\cdot 4H_2O$ (**3**) and the daughter phase **1**:

$$\begin{pmatrix} -1/3 & 0 & 1/3 \\ 0 & -1 & 0 \\ 2/3 & 0 & 1/3 \end{pmatrix} \begin{pmatrix} \boldsymbol{a_3} \\ \boldsymbol{b_3} \\ \boldsymbol{c_3} \end{pmatrix} = \begin{pmatrix} \boldsymbol{a_1} \\ \boldsymbol{b_1} \\ \boldsymbol{c_1} \end{pmatrix},$$

where $\boldsymbol{a_1}$, $\boldsymbol{b_1}$, $\boldsymbol{c_1}$ and $\boldsymbol{a_3}$, $\boldsymbol{b_3}$, $\boldsymbol{c_3}$ are sets of unit-cell vectors for **1** and **3**, respectively (Table 1).

The quality of the crystal recovered to 0.1 MPa permitted the SCXRD measurement of lattice dimensions and structure refinement, which revealed monoclinic symmetry of space group $C2/m$ (Table 1, Fig. 2a, also ESI†). The structure was found to be highly pseudo-symmetric (for details see ESI†) and similar to the trigonal structure previously reported for **1**.[30] The two determinations of this layered $[H_3O]_{2x}[Pb_{1-x}I_2]\cdot(2-2x)H_2O$ structure are consistent (Fig. 1a and 2a), except for a somewhat lower $x = 0.20(2)$ value resulting from our least-squares refinement, compared to $x = 0.23$.[30] The difference, we believe, indicates the possibility of **1** to adopt a wider range of Pb : I stoichiometric compositions. The observed highly topotactic transformation[52] from **3** to **1** requires a transition from 1-D to 2-D polyanions, in which some of the water and HI molecules leave the structure, probably by diffusion, while the

Published on 06 Desemba 2023. Downloaded on 08/10/2025 15:51:46.

edge-sharing connectivity of PbI_6-octahedra is preserved in both materials.

Above 1.2 GPa and above 420 K, a clearly distinct pink-coloured crystalline material (Fig. 4a and b) different from compound **3**, is formed. Subsequent SCXRD at 320 K and pressures above 2.05 GPa revealed a 'hidden' polymorph of PbI_2, herein termed β-PbI_2. This novel form of β-PbI_2 (Table 1, Fig. 4c, d, also ESI†) of the monoclinic space group *C*2/*m* and unprecedented for PbI_2 polymorphs exhibits a 3-D framework of alternating six- and seven-coordinated Pb^{2+} cations bridged by iodide ions, in stark contrast to the well-known 2-D layered structure with six-coordinated Pb^{2+} cations herein termed α-PbI_2.[53,54] The β-PbI_2 displays a rare property of reverse solubility, as we observed the growth of β-PbI_2 crystals on increasing the temperature, and their dissolution on cooling of the DAC. The isochoric conditions in the DAC imply that the increased temperature results either in the increased pressure (for the overall positive thermal expansion of all components in the DAC chamber) or the pressure drops (for the overall negative thermal expansion). According to our knowledge on numerous high-pressure crystallizations reported in the literature, the temperature increase always enhanced dissolution of the solid compounds. There are very few compounds becoming less soluble with increasing temperature (*e.g.* Li_2SO_4); likewise, few compounds for which the reverse solubility with the increase of pressure were reported. The formation of β-PbI_2 is consistent with high-pressure effect increasing the coordination numbers due to stronger compression of anions than cations.[42,55,56] Recently, the high-pressure phases (phase II and III) of the 2H-type PbI_2 polytype, first identified by Bridgman *via* isothermal compression,[58,59] were characterized.[57] Phase II (space group *P*3*m*1) crystallizes above 0.58 GPa as a two-dimensional 4H polytype, while in phase III (orthorhombic *Pnma*), stable above 2.6 GPa, each Pb atom is coordinated by 9 I-atoms similarly as in the orthorhombic $PbCl_2$-structure.[57] However, both phases II and III contrast with the complex structure of β-PbI_2, which requires *in situ* recrystallization and cannot be obtained by cooling/heating or compressing another phase; hence β-PbI_2 is referred to as a 'hidden phase'. In this respect, PbI_2 is similar to imidazole where the β phase can be accessed only by high-pressure recrystallization.[60]

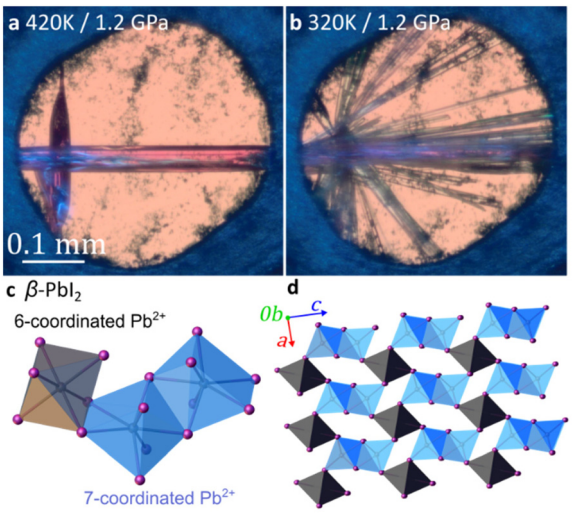

Fig. 4 The 3-D network polymorph of PbI_2. Pink single crystals of β-PbI_2 at 1.2 GPa and: (a) 420 K and (b) 320 K covered by a bundle of needle crystals of **3**. Views of the β-PbI_2 structure: (c) 6- and 7-coordinated Pb^{2+} cations shown in grey and blue, respectively, and (d) the 3-D network viewed along the crystallographic *b*-axis.

Another crystalline phase (**4**) was obtained either by recrystallizing **3** above 1.2 GPa or by spontaneous recrystallization of β-PbI_2 in the DAC below 350 K (Fig. 1d, also ESI†). Below 1.2 GPa, at 320 K, pink β-PbI_2 dissolves and colourless needle-like crystals of **4** appear. Recrystallization by mild temperature oscillation produced a diffraction-quality single crystal of **4** (Fig. 1d and Table 1).

Compound **4** was found to exhibit the formula $(H_3O)PbI_3{\cdot}3H_2O$, again based on polymeric anions with edge-sharing PbI_6-octahedra identical to those in **3** and a variety of lead halide perovskites, but with a lower content of crystallization water. The lower content of water in **4** compared to **3** is consistent with shorter I···I contacts at higher pressure. In the case of compound **4**, also four distinct lengths of Pb–I bonds are present in the anions: 2.81(4), 3.186(12) (twice), 3.232(11) (twice), and 3.34(4) Å. These bond lengths are consistent with lead again adopting the Pb^{2+} oxidation state (Fig. S10†), implying the anion composition PbI_3^-.

In **4**, oxygen atoms of water molecules form ribbons (about 10 Å wide). Within the ribbons shorter hydrogen bonds [O···O distances of 2.73(9) Å] are arranged into three 1-D zigzag chains, interconnected by weaker hydrogen bonds [O···O distance of 3.1(2) Å] into a strongly distorted honeycomb motif. The ribbons separate the adjacent pairs of PbI_3^- polyanions. Additionally, there are also oxygen atoms not involved in any O···O contacts commensurate with hydrogen bonds, but they are each close to iodine atoms of PbI_3^- anions, with O···I distances of 3.187(12) (twice), 3.232(11) (twice), 2.80(4) and 3.33(4) Å, at a pressure of 2.63 GPa and a temperature of 300 K. As indicated above, the hydronium cations and water molecules (Fig. 2c) were discriminated according to the O···PbI_3^- distances, shorter for the charge-assisted OH^+···I bonds.

The appearance of the herein described series of structures comprising the α- and β-forms of PbI_2, as well as hydrated iodoplumbic acids **1**–**4** can be rationalized through the interplay of effects related to the intercalation of HI(aq) and to high-pressure conditions. Specifically, the observation of different structures at different conditions outlines several stability regions in the preference *p*–*T* diagram (Fig. 5), where the low-pressure end-member is α-PbI_2 with a 2-D layer structure, and the high-pressure end-member is β-PbI_2, in which some of the Pb^{2+} cations become 7-coordinated to form a 3-D network.

All members of the series, exhibiting either 1-D, 2-D or 3-D structures, contain the common motif of edge-sharing PbI_6^- octahedra (Fig. 1 and 2), based on Pb–I bonds that are by far and large the least compressed elements constituting the scaffolds of the structures (Table 1). In contrast, the I···I contacts between PbI_2 sheets or the iodoplumbate(II) anions are

 This journal is © the Partner Organisations 2024

Published on 06 Desemba 2023. Downloaded on 08/10/2025 15:51:46.

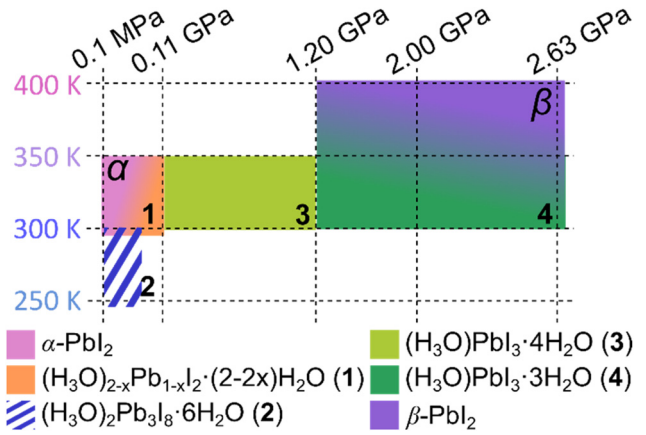

Fig. 5 The *p*/*T* preference diagram for the PbI_2 and HI(aq) system, with the end members being the previously known 2-D α-PbI_2 and the herein reported 3-D β-PbI_2. Acids **1** and **2** are obtained by milling and vapor-solid reactions, whereas **1**, **3**, **4** and β-PbI_2 result from high-pressure synthesis in the DAC.

expected to be considerably weaker and most likely to be affected by pressure, temperature and overall chemical environment. The structures **1–4** can be seen as resulting from the α-PbI_2 structure through intercalation of water and H_3O^+ from HI(aq), resulting in O–H···I bonds between polyanionic sheets and tapes, which prevent their contacts involving iodine atoms.

The observation of compounds **1–3** at pressures up to 1.2 GPa occurs by progressive insertion of hydronium ions from HI(aq) into the PbI_2 structure, leading to the formation of an anion with PbI_3^- composition. At 1.2 GPa a partial desorption of water is observed, leading to the formation of compound **4** that maintains the structure and composition of the PbI_3^- anions. This chemical process first requires a dissolution of **3** and it is consistent with our previous general observation that recrystallizations conducted above 1 GPa often destabilize hydrates.[60–62] Ultimately, exposing the system to still higher pressure and temperature completely prevents water intercalation into the structure of PbI_2 and leads to the formation of a 3-D structure through creation of new Pb–I bonds and 7-coordinated lead(II) ions.

The effect of temperature and pressure on the aqueous solutions of α-PbI_2 and HI can be represented in the chemical formula reported by Daub and Hillebrecht:[30] $(H_2O)_\delta(PbI_2)_\varepsilon(HI)_\zeta$.

According to this formula, the stoichiometry of compounds **1–4** can be represented as:

Compound **1** $(H_2O)_{2.597}(PbI_2)(HI)_{0.597}$ for $x = 0.23$ [ref. 30]

Compound **1′** $(H_2O)_{2.5}(PbI_2)(HI)_{0.5}$ for $x = 0.20$ [this work]

Compound **2** $(H_2O)_{2.667}(PbI_2)(HI)_{0.667}$ [ref. 30 & this work]

Compound **3** $(H_2O)_5(PbI_2)(HI)$ [this work]

Compound **4** $(H_2O)_4(PbI_2)(HI)$ [this work],

where x is the Pb^{2+} deficit parameter.[30] The formulae above illustrate the stoichiometric relations observed for the syntheses of compounds **1**, **2**, **3** and **4**. When related to the amount of PbI_2 in the ambient-pressure compounds **1** and **2**, the number of moles of HI and of H_2O is higher in **3** and **4**, which can be rationalized by a smaller compression of the Pb–I bonded polyanionic skeletons, compared to considerably softer OH···O and OH···I interactions. Consequently, more water molecules are needed for separating the polyanions. On the transition from **3** to **4**, the polyanions are compressed closer, their separation decreases and the space available for the corrugated layers of H-bonded H_2O and $[H_3O]^+$ is reduced. This reduced space can accommodate fewer H_2O molecules in **4**, whereas the contents of hydronium cations H_3O^+ equilibrate the charge of the polyanions through the neutral-charge condition. The above formulae also illustrate that more HI is needed for the formation of high-pressure products **3** and **4** compared to the gas-phase reaction leading to compound **2**. Under ambient conditions, the increased presence of HI leads to the formation of ribbon polyanions in **2** capable of accommodating more H_2O molecules and H_3O^+ cations around them, compared to the layer polyanions formed in **1**. In the reaction to compound **3**, the higher pressure decreases the distances and further increases electrostatic interactions, which in turn can be better stabilized by compressed contacts between I^- anions and H_3O^+ cations. These charge-assisted contacts are shorter by about 0.5 Å compared to those in ambient-pressure compound **2**. Accordingly, the formation of smaller polyanions increases the surface where the negative charge is distributed on terminal I atoms, hence resulting in the presence of wider triple-chain polyanionic ribbons $[Pb_3I_8]_n^{2-}$ in **2** and narrower double-chain polyanionic ribbons $[Pb_2I_6]_n^{2-}$ in **3** and **4**.

The herein observed structures of hydrated iodoplumbic acids **1–4** resemble some of those recently observed for solvates of popular methylammonium ($CH_3NH_3^+$) and formamidinium ($CH(NH_2)_2^+$) iodoplumbates with *N*,*N*-dimethylformamide (DMF), *S*,*S*-dimethylsulfoxide (DMSO) and/or water.[49] Such solvates have attracted significant attention as intermediates in the formation,[63–65] or products of moisture-induced degradation, of hybrid perovskite thin films highlighting the importance of the current findings.[66,67] Specifically, structures containing polymeric $Pb_3I_8^{2-}$ anions, reminiscent of the ones found in **2**, were observed as solvates for both methylammonium and formamidinium iodoplumbate with DMF,[68,69] and in the former case also in a solvate with DMSO.[70] While the PbI_3^- anionic double-chain motifs observed in **3** and **4** are also found in several hydrates of alkaline metal iodoplumbates (II), it is also found in the hydrate and an alternative DMF solvate of $CH_3NH_3PbI_3$.[49,69] In these two structures, the anionic PbI_3^- double chains are aligned in parallel and separated by protonated cations and solvent molecules (water, DMF), and form arrangements broadly similar to the crystal structures of **3** and **4**, where the anions also lie aligned in parallel and are separated by hydronium cations and water molecules. However, compounds **3** and **4** are not strictly isostructural to any of these previously reported solvated structures.

Other types of anions, not yet observed in our high-pressure studies, have been observed in solvated forms of methyl-

Published on 06 Desemba 2023. Downloaded on 08/10/2025 15:51:46.

ammonium and formamidinium iodoplumbates, notably a dihydrate of the methylammonium salt based on monomeric octahedral PbI_6^{4-} ions,[71] as well as DMF[72] and DMSO[73] solvates of the methylammonium salts containing polymeric PbI_5^- anions composed of corner-sharing PbI_6-octahedra. Importantly in the context of the present work, the crystal structure[68] of the DMF solvate of $CH(NH_2)_2PbI_3$ presents an alternative form of the PbI_3^- anion, in the form of simple chains formed by face-sharing PbI_6-octahedra. While our studies have so far not revealed any evidence for such a phase based on hydronium ions, we believe they suggest the possibility of another, structurally distinct, class of iodoplumbic acid hydrates.

Conclusion

In summary, high-energy isochoric syntheses in a DAC revealed the first structures of the so far elusive and controversial iodoplumbic acid, in the form of a hydrated hydronium salts of $[PbI_3]^-$ achievable at elevated temperature and pressure, providing new experimental information relevant for the previous speculations regarding possible $HPbI_3$ structure. In that respect, the iodoplumbic acids synthesized under high-pressure resemble other inorganic acids that are known only in the hydrated from, such as $HAuCl_4$ or $HICl_4$.[74,75] The herein obtained hydronium-based acids are based on 1-D double-chain of composition PbI_3^- anions, analogous to those found in the archetypal, well-known lead perovskites $RbPbI_3$, $CsPbI_3$, $NH_4PbI_3{\cdot}2H_2O$, or $CsPbI_3{\cdot}2H_2O$.[44–48] The composition and structure of anions distinguish these high-pressure materials from iodoplumbic acids made by recrystallization of PbI_2 from aqueous hydriodic acid,[30] and render them the so far first observed examples of iodoplumbic acid: a material of fundamental significance as the formal inorganic progenitor of the highly popular class of hybrid perovskite materials. The herein described series of hydrated iodoplumbic acids constitutes a family of closely related compounds with those previously reported at standard pressure,[30] and their high-pressure synthesis can be described through the following equations:

$$\alpha - PbI_2 + \text{conc. } HI_{(aq)} \xrightarrow{p>0.1\,\text{GPa}} (H_3O)PbI_3 \cdot 4H_2O (\text{compound } \mathbf{3})$$

$$(H_3O)PbI_3 \cdot 4H_2O \xrightarrow{p>1.2\,\text{GPa}} (H_3O)PbI_3 \cdot 3H_2O (\text{compound } \mathbf{4})$$

$$(H_3O)PbI_3 \cdot 3H_2O \xrightarrow{\Delta, p>2.0\,\text{GPa}} \beta - PbI_2 + HI_{(aq)}$$

These processes can be rationalized through intercalation of water molecules and hydronium ions between negatively charged lead iodide fragments, resulting in O–H···I and $O–H^+\cdots I^{\delta-}$ hydrogen bonds that reduce electrostatic repulsion and prevent close contacts between the anions. This system exhibits high sensitivity to external stimuli, as evidenced by the observation of so far four iodoplumbic acids, up to high pressures (>2 GPa) and temperatures (>350 K) at which intercalation is no longer favoured and a new form of lead(II) iodide (β-PbI_2) appears (see the equation above). The β-PbI_2 structure is the unique polymorph of lead(II) iodide and, in contrast to the previously reported phases,[57] it is based on the 3-dimensional network of edge-sharing PbI_6 and PbI_7 octahedra.

Overall, this work provides new fundamental chemical information about lead-iodide perovskite solids, viewed from the perspective of high-pressure and high-temperature conditions. The role of investigated PbI_2/HI(aq) system as a key intermediate in the synthesis of perovskite-based solar cells and its use as a model for probing novel perovskite materials can unveil novel pathways in the renewable energy industry. This exploration underscores the criticality of further research into iodoplumbic-based materials applications, potentially catalysing breakthroughs in the design and performance of next-generation photovoltaic technologies. In line with the high potential of high-pressure techniques in generating new material structures,[39,40,42,76] this work highlights crystallization from the high-energy DAC environment as a simple and straightforward means to discover new phases, even in compositionally simple systems such as PbI_2 that has been extensively studied[53,54] for almost a century. Whereas the herein described structures of hydrated iodoplumbic acids are so far accessible only at high pressures, and therefore not of immediate importance for the construction of devices, they provide a fundamental advance in the understanding of this important family of materials and a new high-pressure perspective revealing unexpected structures important for the debate on the existence of iodoplumbic acids.

Experimental section

High-pressure experiments

For the high-pressure experiments a liquid solution of PbI_2 dissolved in concentrated aqueous hydroiodic acid (HI, 57% by weight) was loaded to a modified Merrill-Bassett diamond anvil cell (DAC). The DAC anvils were supported directly on the steel discs with conical windows (the culet size was 0.8 mm, type 1A diamonds and gasket was made of 0.15 mm thick austenitic steel (type 25-6MO) with the hole diameter 0.45 mm).[41] Pressure in the DAC was determined by the ruby fluorescence (R1 ruby line) shift with a photon control spectrometer affording an accuracy of 0.02 GPa.[77] Throughout all experiments, the hydrostatic conditions in the DAC were routinely inspected visually by microscopic observations (*cf.* General microscopy in ESI† for details), by checking the width of the R1 and R2 ruby fluorescence peaks and the widths of SCXRD reflections as well as by searching the background of X-ray images for the presence of diffraction events other than those from the sample crystal. By these means we can be confident that all experiments were conducted in hydrostatic conditions. We attempted high-pressure syntheses and recrystallizations above 3 GPa, however most of the DAC chamber contents froze and its melting required the temperatures approaching the re-

 This journal is © the Partner Organisations 2024

Published on 06 Desemba 2023. Downloaded on 08/10/2025 15:51:46.

sistance of the steel parts of the DAC and caused difficulties in controlling precisely the temperature and pressure, as required for the growth of single crystals.

Diffraction data were collected at 295 K for **1**, **3** and **4** and at 320 K for β-PbI_2, by using a KM-4 CCD diffractometer with the graphite-monochromated MoK_α radiation. The DAC was centered by the gasket-shadow method.[78] The CrysAlisCCD and CrysAlisRED programs were used for collecting the data, determination of the UB-matrices, initial data reduction, and L_p correction. Reflection intensities were corrected for the DAC and sample absorption; the gasket shadowing and the reflections of diamond-anvils were eliminated.[79] All structures were solved by direct methods, and refined with anisotropic displacement parameters, with programs ShelXS and ShelXL using Olex2 interface.[80,81] For re-determination of the structure of **1**, the positions of water hydrogen atoms were estimated from the molecular geometry and consistently with the pseudo-hexagonal hydrogen-bonding pattern in the structure. The water molecules were then refined using a rigid-group model, with the isotropic temperature factors of the hydrogen atoms (U_{iso}) constrained to be 1.5 times the U_{eq} of the corresponding oxygen atom. Details of structure refinements and crystal data are given in Table S1.† Crystallographic data in CIF format have been deposited with the Cambridge Structural Data Centre, under deposition codes 2071140–2071144.†

High-pressure synthesis of 3 & 4

Single crystals of **3** and **4** were obtained in isochoric conditions: after the polycrystalline mass precipitated, the DAC was heated using a heat gun until all but one grain dissolved. Then the single crystal grew as the DAC was cooled slowly to room temperature, where the pressure was remeasured before and after the X-ray diffraction experiment. The progress and experimental details on growing the single crystals of **3** and **4** are shown in Fig. S1 and S2.†

High-pressure synthesis of β-PbI_2

Single crystals of β-PbI_2 were obtained similarly to those of **3** and **4**, however due to the phase transformation at room temperature at 1.2 GPa, the single crystal grown at 2.05 GPa was kept at 320 K and the X-ray diffraction experiment was performed at this temperature.

Ball milling experiments

*Milling synthesis of **1***: For the ball milling synthesis, 0.461 g (1 mmol) of PbI_2 was added to one half of a zirconia (ZrO_2) 10 mL jar, followed by the addition of 67 μL (0.5 mmol) of aqueous hydroiodic acid (HI, 57% by weight) and one 3.5 g zirconia ball. The jar was carefully sealed, placed on a MM400 mixer mill and the reaction mixture was milled for 30 minutes at a frequency of 30 Hz. Reaction completion afforded a bright yellow product, which was left to dry in dark for 1 h. The resulting solid product was scraped off the jar walls and subjected to powder X-ray diffraction (PXRD) analysis, revealing the formation of compound **1**. Compound **1** can be also isolated when performing the 1 : 1 stoichiometric reaction by milling 0.230 g (0.5 mmol) of PbI_2 with 67 μL (0.5 mmol) of aqueous hydroiodic acid (HI, 57% by weight), respectively. *Milling synthesis of **2***: For the ball-milling synthesis 0.230 g (0.5 mmol) of PbI_2 was added to one half of a zirconia (ZrO_2) 10 mL jar, followed by the addition of 201 μL (1.5 mmol) of aqueous hydroiodic acid (HI, 57% by weight) and one 3.5 g zirconia ball. The jar was carefully sealed and placed on a MM400 mixer mill and the reaction mixture was milled for 30 minutes at an oscillation rate of 30 Hz. Reaction completion afforded a bright yellow product, which was left to dry in dark overnight. The resulting product scraped off the jar walls was identified as compound **2** by PXRD.

Data availability

Description of pseudosymmetry in **1**, experimental procedures and detailed crystallographic data of **3**, **4** and β-PbI_2, ball-milling experiments, and additional data are located within the ESI.†

Author contributions

All high-pressure experiments were performed by S. S., ball milling by A. M. F. and J.-L. D. Research was coordinated and supervised by A. K., T. F., A. M. and G. P. D. All authors discussed the results, contributed to writing the manuscript and commented on it.

Conflicts of interest

The authors declare no conflict of interest.

Acknowledgements

We acknowledge the McGill Sustainability Systems Initiative (MSSI) and NSERC Discovery Grant program. S. S. is grateful to the grant POWR.03.02.00-00-I023/17 co-financed by the European Union through the European Social Fund under the Operational Program Knowledge Education Development.

References

1 J. Euvrard, Y. Yan and D. B. Mitzi, Electrical doping in halide perovskites, *Nat. Rev. Mater.*, 2021, **6**, 531–549.
2 S. D. Stranks and H. J. Snaith, Metal-halide perovskites for photovoltaic and light-emitting devices, *Nat. Nanotechnol.*, 2015, **10**, 391–402.
3 L.-Q. Fan and J.-H. Wu, NH_4PbI_3, *Acta Crystallogr., Sect. E: Struct. Rep. Online*, 2007, **63**, i189–i189.
4 J. Burschka, N. Pellet, S. J. Moon, R. Humphry-Baker, P. Gao, M. K. Nazeeruddin and M. Grätzel, Sequential

Published on 06 Desemba 2023. Downloaded on 08/10/2025 15:51:46.

deposition as a route to high-performance perovskite-sensitized solar cells, *Nature*, 2013, **499**, 316–319.

5 N. J. Jeon, J. H. Noh, Y. C. Kim, W. S. Yang, S. Ryu and S. Il Seok, Solvent engineering for high-performance inorganic–organic hybrid perovskite solar cells, *Nat. Mater.*, 2014, **13**, 897–903.

6 S. Huang, P. Huang, L. Wang, J. Han, Y. Chen and H. Zhong, Halogenated–Methylammonium Based 3D Halide Perovskites, *Adv. Mater.*, 2019, **31**, 1903830.

7 M. Szafrański and A. Katrusiak, Mechanism of pressure-induced phase transitions, amorphization, and absorption-edge shift in photovoltaic methylammonium lead iodide, *J. Phys. Chem. Lett.*, 2016, **7**, 3458–3466.

8 M. Szafrański and A. Katrusiak, Photovoltaic hybrid perovskites under pressure, *J. Phys. Chem. Lett.*, 2017, **8**, 2496–2506.

9 M. Shirayama, H. Kadowaki, T. Miyadera, T. Sugita, M. Tamakoshi, M. Kato, T. Fujiseki, D. Murata, S. Hara, T. N. Murakami, S. Fujimoto, M. Chikamatsu and H. Fujiwara, Optical Transitions in Hybrid Perovskite Solar Cells: Ellipsometry, Density Functional Theory, and Quantum Efficiency Analyses for $CH_3NH_3PbI_3$, *Phys. Rev. Appl.*, 2016, **5**, 1–25.

10 D. Prochowicz, R. Runjhun, M. M. Tavakoli, P. Yadav, M. Saski, A. Q. Alanazi, D. J. Kubicki, Z. Kaszkur, S. M. Zakeeruddin, J. Lewiński and M. Grätzel, Engineering of perovskite materials based on formamidinium and cesium hybridization for high-efficiency solar cells, *Chem. Mater.*, 2019, **31**, 1620–1627.

11 Y. Wang, M. I. Dar, L. K. Ono, T. Zhang, M. Kan, Y. Li, L. Zhang, X. Wang, Y. Yang, X. Gao, Y. Qi, M. Grätzel and Y. Zhao, Thermodynamically stabilized β-$CsPbI_3$-based perovskite solar cells with efficiencies >18%, *Science*, 2019, **365**, 591–595.

12 W. Ahmad, J. Khan, G. Niu and J. Tang, Inorganic $CsPbI_3$ Perovskite–Based Solar Cells: A Choice for a Tandem Device, *Sol. RRL*, 2017, **1**, 1–9.

13 T. Baikie, Y. Fang, J. M. Kadro, M. Schreyer, F. Wei, S. G. Mhaisalkar, M. Graetzel and T. J. White, Synthesis and crystal chemistry of the hybrid perovskite $(CH_3NH_3)PbI_3$ for solid-state sensitised solar cell applications, *J. Mater. Chem. A*, 2013, **1**, 5628–5641.

14 D. Prochowicz, M. Franckevičius, A. M. Cieślak, S. M. Zakeeruddin, M. Grätzel and J. Lewiński, Mechanosynthesis of the hybrid perovskite $CH_3NH_3PbI_3$: characterization and the corresponding solar cell efficiency, *J. Mater. Chem. A*, 2015, **3**, 20772–20777.

15 D. Prochowicz, P. Yadav, M. Saliba, M. Saski, S. M. Zakeeruddin, J. Lewiński and M. Grätzel, Mechanosynthesis of pure phase mixed-cation $MA_xFA_{1-x}PbI_3$ hybrid perovskites: photovoltaic performance and electrochemical properties, *Sustainable Energy Fuels*, 2017, **1**, 689–693.

16 W. Huang, J. S. Manser, S. Sadhu, P. V. Kamat and S. Ptasinska, Direct Observation of Reversible Transformation of $CH_3NH_3PbI_3$ and NH_4PbI_3 Induced by Polar Gaseous Molecules, *J. Phys. Chem. Lett.*, 2016, **7**, 5068–5073.

17 A. Jain, S. P. Ong, G. Hautier, W. Chen, W. D. Richards, S. Dacek, S. Cholia, D. Gunter, D. Skinner, G. Ceder and K. A. Persson, Commentary: The Materials Project: A materials genome approach to accelerating materials innovation, *APL Mater.*, 2013, **1**, 011002.

18 F. Wang, H. Yu, H. Xu and N. Zhao, $HPbI_3$: A New Precursor Compound for Highly Efficient Solution–Processed Perovskite Solar Cells, *Adv. Funct. Mater.*, 2015, **25**, 1120–1126.

19 S. Pang, Y. Zhou, Z. Wang, M. Yang, A. R. Krause, Z. Zhou, K. Zhu, N. P. Padture and G. Cui, Transformative Evolution of Organolead Triiodide Perovskite Thin Films from Strong Room-Temperature Solid–Gas Interaction between $HPbI_3$-CH_3NH_2 Precursor Pair, *J. Am. Chem. Soc.*, 2016, **138**, 750–753.

20 Z. Zhou, S. Pang, F. Ji, B. Zhang and G. Cui, The fabrication of formamidinium lead iodide perovskite thin films via organic cation exchange, *Chem. Commun.*, 2016, **52**, 3828–3831.

21 M. Long, T. Zhang, Y. Chai, C. F. Ng, T. C. W. Mak, J. Xu and K. Yan, Nonstoichiometric acid–base reaction as reliable synthetic route to highly stable $CH_3NH_3PbI_3$ perovskite film, *Nat. Commun.*, 2016, **7**, 1–11.

22 M. Long, T. Zhang, H. Zhu, G. Li, F. Wang, W. Guo, Y. Chai, W. Chen, Q. Li, K. S. Wong, J. Xu and K. Yan, Textured $CH_3NH_3PbI_3$ thin film with enhanced stability for high performance perovskite solar cells, *Nano Energy*, 2017, **33**, 485–496.

23 F. Ji, S. Pang, L. Zhang, Y. Zong, G. Cui, N. P. Padture and Y. Zhou, Simultaneous Evolution of Uniaxially Oriented Grains and Ultralow-Density Grain-Boundary Network in $CH_3NH_3PbI_3$ Perovskite Thin Films Mediated by Precursor Phase Metastability, *ACS Energy Lett.*, 2017, **2**, 2727–2733.

24 Y. Wei, W. Li, S. Xiang, J. Liu, H. Liu, L. Zhu and H. Chen, Precursor effects on methylamine gas-induced $CH_3NH_3PbI_3$ films for stable carbon-based perovskite solar cells, *Sol. Energy*, 2018, **174**, 139–148.

25 X. Ding, H. Chen, Y. Wu, S. Ma, S. Dai, S. Yang and J. Zhu, Triple cation additive $NH_3{}^+C_2H_4NH2{}^+C_2H_4NH_3{}^+$-induced phase-stable inorganic α-$CsPbI_3$ perovskite films for use in solar cells, *J. Mater. Chem. A*, 2018, **6**, 18258–18266.

26 Z. Liu, L. Qiu, E. J. Juarez-Perez, Z. Hawash, T. Kim, Y. Jiang, Z. Wu, S. R. Raga, L. K. Ono, S. (Frank) Liu and Y. Qi, Gas-solid reaction based over one-micrometer thick stable perovskite films for efficient solar cells and modules, *Nat. Commun.*, 2018, **9**, 1–11.

27 T. Zhang, M. I. Dar, G. Li, F. Xu, N. Guo, M. Grätzel and Y. Zhao, Bication lead iodide 2D perovskite component to stabilize inorganic α-$CsPbI_3$ perovskite phase for high-efficiency solar cells, *Sci. Adv.*, 2017, **3**, 1–7.

28 S. A. Fateev, E. I. Marchenko, A. A. Petrov, E. A. Goodilin and A. B. Tarasov, New Acidic Precursor and Acetone-Based Solvent for Fast Perovskite Processing via Proton-Exchange Reaction with Methylamine, *Molecules*, 2020, **25**, 1856.

 This journal is © the Partner Organisations 2024

Published on 06 Desemba 2023. Downloaded on 08/10/2025 15:51:46.

29 W. Ke, I. Spanopoulos, C. C. Stoumpos and M. G. Kanatzidis, Myths and reality of $HPbI_3$ in halide perovskite solar cells, *Nat. Commun.*, 2018, **9**, 4785.
30 M. Daub and H. Hillebrecht, On the Demystification of "$HPbI_3$" and the Peculiarities of the Non–innocent Solvents H_2O and DMF, *Z. Anorg. Allg. Chem.*, 2018, **644**, 1393–1400.
31 D. Prochowicz, M. Saski, P. Yadav, M. Grätzel and J. Lewiński, Mechanoperovskites for photovoltaic applications: preparation, characterization, and device fabrication, *Acc. Chem. Res.*, 2019, **52**, 3233–3243.
32 Z. Hong, D. Tan, R. A. John, Y. K. E. Tay, Y. K. T. Ho, X. Zhao, T. C. Sum, N. Mathews, F. García and H. S. Soo, Completely solvent-free protocols to access phase-pure, metastable metal halide perovskites and functional photodetectors from the precursor salts, *iScience*, 2019, **16**, 312–325.
33 T. Friščić, C. Mottillo and H. M. Titi, Mechanochemistry for synthesis, *Angew. Chem., Int. Ed.*, 2020, **59**, 1018–1029.
34 S. A. Moggach, T. D. Bennett and A. K. Cheetham, The effect of pressure on ZIF–8: increasing pore size with pressure and the formation of a high–pressure phase at 1.47 GPa, *Angew. Chem., Int. Ed.*, 2009, **48**, 7087–7089.
35 J. Song, R. Pallach, L. Frentzel-Beyme, P. Kolodzeiski, G. Kieslich, P. Vervoorts, C. L. Hobday and S. Henke, Tuning the High-Pressure Phase Behaviour of Highly Compressible Zeolitic Imidazolate Frameworks: From Discontinuous to Continuous Pore Closure by Linker Substitution, *Angew. Chem., Int. Ed.*, 2022, **61**, e202117565.
36 S. Sun, Z. Deng, Y. Wu, F. Wei, F. H. Isikgor, F. Brivio, M. W. Gaultois, J. Ouyang, P. D. Bristowe, A. K. Cheetham and G. Kieslich, Variable temperature and high-pressure crystal chemistry of perovskite formamidinium lead iodide: a single crystal X-ray diffraction and computational study, *Chem. Commun.*, 2017, **53**, 7537–7540.
37 L. Zhang, L. Wu, K. Wang and B. Zou, Pressure-Induced Broadband Emission of 2D Organic–Inorganic Hybrid Perovskite $(C_6H_5C_2H_4NH_3)_2PbBr_4$, *Adv. Sci.*, 2019, **6**, 2–7.
38 S. Sobczak, P. Ratajczyk and A. Katrusiak, Squeezing Out the Catalysts: A Sustainable Approach to Disulfide Bond Exchange in Aryl Disulfides, *ACS Sustainable Chem. Eng.*, 2021, **9**, 7171–7178.
39 S. Sobczak and A. Katrusiak, Environment-Controlled Postsynthetic Modifications of Iron Formate Frameworks, *Inorg. Chem.*, 2019, **58**, 11773–11781.
40 A. Katrusiak, Lab in a DAC–high-pressure crystal chemistry in a diamond-anvil cell, *Acta Crystallogr., Sect. B: Struct. Sci., Cryst. Eng. Mater.*, 2019, **75**, 918–926.
41 A. Katrusiak, High-pressure devices, in *International Tables for Crystallography Volume H*, ed. C. J. Gilmore, J. A. Kaduk and H. Schenk, John Wiley & Sons, Inc., New York, 2018, pp. 156–173.
42 W. Grochala, R. Hoffmann, J. Feng and N. W. Ashcroft, The Chemical Imagination at Work in Very Tight Places, *Angew. Chem., Int. Ed.*, 2007, **46**, 3620–3642.
43 M. Szafrański and A. Katrusiak, Phase transitions in layered diguanidinium hexachlorostannate (IV), *Phys. Rev. B: Condens. Matter Mater. Phys.*, 2000, **61**, 1026–1035.
44 H. Brasseur and L. Pauling, The Crystal Structure of Ammonium Cadmium Chloride, NH_4CdCl_3, *J. Am. Chem. Soc.*, 1938, **60**, 2886–2890.
45 D. Bedlivy and K. Mereiter, The structures of potassium lead triiodide dihydrate and ammonium lead triiodide dihydrate, *Acta Crystallogr., Sect. B: Struct. Crystallogr. Cryst. Chem.*, 1980, **36**, 782–785.
46 C. K. Møller, Crystal Structure and Photoconductivity of Cæsium Plumbohalides, *Nature*, 1958, **182**, 1436–1436.
47 H. J. Haupt, F. Huber and H. Preut, Darstellung und Kristallstruktur von Rubidiumtrijodoplumbat(II), *Z. Anorg. Allg. Chem.*, 1974, **408**, 209–213.
48 D. M. Trots and S. V. Myagkota, High-temperature structural evolution of caesium and rubidium triiodoplumbates, *J. Phys. Chem. Solids*, 2008, **69**, 2520–2526.
49 F. Hao, C. C. Stoumpos, Z. Liu, R. P. H. Chang and M. G. Kanatzidis, Controllable perovskite crystallization at a gas–solid interface for hole conductor-free solar cells with steady power conversion efficiency over 10%, *J. Am. Chem. Soc.*, 2014, **136**, 16411–16419.
50 S. Alvarez, A cartography of the van der Waals territories, *Dalton Trans.*, 2013, **42**, 8617–8636.
51 P. Gilli, L. Pretto, V. Bertolasi and G. Gilli, Predicting Hydrogen-Bond Strengths from Acid–Base Molecular Properties. The pK_a Slide Rule: Toward the Solution of a Long-Lasting Problem, *Acc. Chem. Res.*, 2009, **42**, 33–44.
52 J. M. Thomas, Topography and topology in solid-state chemistry, *Philos. Trans. R. Soc., A*, 1974, **277**, 251–286.
53 P. Terpstra and H. G. Westenbrink, Organic Cation Substitution in Hybrid Perovskite $CH_3NH_3PbI_3$ with Hydroxylammonium (NH_3OH^+): A First-Principles Study, *Proc. K. Ned. Acad. van Wet.*, 1926, **29**, 431–442.
54 P. A. Beckmann, A review of polytypism in lead iodide, *Cryst. Res. Technol.*, 2010, **45**, 455–460.
55 C. T. Prewitt and R. T. Downs, *Rev. Mineral.*, 1998, **37**, 283 ("high-pressure crystal chemistry").
56 A. Półrolniczak, S. Sobczak and A. Katrusiak, Solid-state associative reactions and the coordination compression mechanism, *Inorg. Chem.*, 2018, **57**, 8942–8950.
57 J. F. Ding, P. Cheng, T. T. Ye, W. Xu, H. Zeng, D. Y. Yao, X. M. Pan and J. Zhang, Pressure-Induced Bifurcation in the Photoluminescence of Red Carbon Quantum Dots: Coexistence of Emissions from Surface Groups and Nitrogen-Doped Cores, *Appl. Phys. Lett.*, 2022, **120**, 052106.
58 P. W. Bridgman, Polymorphic Transitions of 35 Substances to 50,000 Kg/cm^3, *Proc. Am. Acad. Arts Sci.*, 1937, **72**, 45.
59 P. W. Bridgman, Rough Compressions of 177 Substances to 40,000 Kg/cm^3, *Proc. Am. Acad. Arts Sci.*, 1948, **76**, 71.
60 D. Paliwoda, K. F. Dziubek and A. Katrusiak, Imidazole Hidden Polar Phase, *Cryst. Growth Des.*, 2012, **12**, 4302–4430.

Published on 06 Desemba 2023. Downloaded on 08/10/2025 15:51:46.

61 H. Tomkowiak, A. Olejniczak and A. Katrusiak, Pressure-Dependent Formation and Decomposition of Thiourea Hydrates, *Cryst. Growth Des.*, 2013, **13**, 121–125.
62 F. P. A. Fabbiani, D. R. Allan, W. I. F. David, S. A. Moggach, S. Parsons and C. R. Pulham, High-pressure recrystallisation—a route to new polymorphs and solvates, *CrystEngComm*, 2004, **6**, 504–511.
63 J. W. Lee, H. S. Kim and N. G. Park, Lewis Acid–Base Adduct Approach for High Efficiency Perovskite Solar Cells, *Acc. Chem. Res.*, 2016, **49**, 311–319.
64 D.-K. Lee, K.-S. Lim, J.-W. Lee and N.-G. Park, Scalable perovskite coating via anti-solvent-free Lewis acid–base adduct engineering for efficient perovskite solar modules, *J. Mater. Chem. A*, 2021, **9**, 3018–3028.
65 A. A. Petrov, N. Pellet, J. Y. Seo, N. A. Belich, D. Y. Kovalev, A. V. Shevelkov, E. A. Goodilin, S. M. Zakeeruddin, A. B. Tarasov and M. Graetzel, New Insight into the Formation of Hybrid Perovskite Nanowires Via Structure Directing Adducts, *Chem. Mater.*, 2017, **29**, 587–594.
66 A. M. A. Leguy, Y. Hu, M. Campoy-Quiles, M. I. Alonso, O. J. Weber, P. Azarhoosh, M. Van Schilfgaarde, M. T. Weller, T. Bein, J. Nelson, P. Docampo and P. R. F. Barnes, Reversible Hydration of $CH_3NH_3PbI_3$ in Films, Single Crystals, and Solar Cells, *Chem. Mater.*, 2015, **27**, 3397–3407.
67 D. Li, S. A. Bretschneider, V. W. Bergmann, I. M. Hermes, J. Mars, A. Klasen, H. Lu, W. Tremel, M. Mezger, H. J. Butt, S. A. L. Weber and R. Berger, Humidity-Induced Grain Boundaries in MAPbI3 Perovskite Films, *J. Phys. Chem. C*, 2016, **120**, 6363–6368.
68 A. A. Petrov, S. A. Fateev, V. N. Khrustalev, Y. Li, P. V. Dorovatovskii, Y. V. Zubavichus, E. A. Goodilin and A. B. Tarasov, Formamidinium haloplumbate intermediates: the missing link in a chain of hybrid perovskites crystallization, *Chem. Mater.*, 2020, **32**, 7739–7745.
69 A. A. Petrov, I. P. Sokolova, N. A. Belich, G. S. Peters, P. V. Dorovatovskii, Y. V. Zubavichus, V. N. Khrustalev, A. V. Petrov, M. Grätzel, E. A. Goodilin and A. B. Tarasov, Crystal Structure of DMF-Intermediate Phases Uncovers the Link Between $CH_3NH_3PbI_3$ Morphology and Precursor Stoichiometry, *J. Phys. Chem. C*, 2017, **121**, 20739–20743.
70 Y. Guo, K. Shoyama, W. Sato, Y. Matsuo, K. Inoue, K. Harano, C. Liu, H. Tanaka and E. Nakamura, Chemical Pathways Connecting Lead(II) Iodide and Perovskite via Polymeric Plumbate(II) Fiber, *J. Am. Chem. Soc.*, 2015, **137**, 15907–15914.
71 B. R. Vincent, K. N. Robertson, T. S. Cameron and O. Knop, Alkylammonium lead halides. Part 1. Isolated PbI_6^{4-} ions in $(CH_3NH_3)_4PbI_6{\cdot}2H_2O$, *Can. J. Chem.*, 1987, **65**, 1042–1046.
72 J. Cao, X. Jing, J. Yan, C. Hu, R. Chen, J. Yin, J. Li and N. Zheng, Identifying the molecular structures of intermediates for optimizing the fabrication of high-quality perovskite films, *J. Am. Chem. Soc.*, 2016, **138**, 9919–9926.
73 H. W. Cremer and D. R. Duncan, CCXLIX.—A study of the polyhalides. Part I. Methods of preparation, *J. Chem. Soc.*, 1931, 1857–1866.
74 J. M. Williams and S. W. Peterson, Example of the $[H_5O_2]^+$ ion. Neutron diffraction study of tetrachloroauric acid tetrahydrate, *J. Am. Chem. Soc.*, 1969, **91**, 776–777.
75 J. Cao, X. Jing, J. Yan, C. Hu, R. Chen, J. Yin, J. Li and N. Zheng, Identifying the molecular structures of intermediates for optimizing the fabrication of high-quality perovskite films, *J. Am. Chem. Soc.*, 2016, **138**, 9919–9926.
76 X. Dong, A. R. Oganov, A. F. Goncharov, E. Stavrou, S. Lobanov, G. Saleh, G. R. Qian, Q. Zhu, C. Gatti, V. L. Deringer, R. Dronskowski, X. F. Zhou, V. B. Prakapenka, Z. Konôpková, I. A. Popov, A. I. Boldyrev and H. T. Wang, A stable compound of helium and sodium at high pressure, *Nat. Chem.*, 2017, **9**, 440–445.
77 G. J. Piermarini, S. Block, J. D. Barnett and R. A. Forman, Calibration of the pressure dependence of the R1 ruby fluorescence line to 195 kbar, *J. Appl. Phys.*, 1975, **46**, 2774–2780.
78 A. Budzianowski and A. Katrusiak, in *High-Pressure Crystallog*, Springer Netherlands, Dordrecht, 2004, pp. 101–112.
79 A. Katrusiak, Shadowing and absorption corrections of single-crystal high-pressure data, *Z. Kristallogr. – Cryst. Mater.*, 2004, **219**, 461–467.
80 G. M. Sheldrick, Crystal Structure Refinement with SHELXL, *Acta Crystallogr., Sect. C: Struct. Chem.*, 2015, **71**, 3–8.
81 O. V. Dolomanov, L. J. Bourhis, R. J. Gildea, J. A. K. Howard and H. Puschmann, OLEX2: A Complete Structure Solution, Refinement and Analysis Program, *J. Appl. Crystallogr.*, 2009, **42**, 339–341.

 This journal is © the Partner Organisations 2024